8/21/2016- Revised

Temperature-robust neural function from activity dependent ion channel regulation

Timothy O'Leary[1] and Eve Marder[2]

Affiliations

1. Department of Engineering, University of Cambridge, Trumpington St, Cambridge CB2 1PZ, United Kingdom
2. Volen Center for Complex Systems, Brandeis University, Waltham MA 02454, USA

Email addresses

timothy.oleary@eng.cam.ac.uk

marder@brandeis.edu

Highlights

- Neural activity is generically highly temperature sensitive
- Neurons achieve temperature robustness with highly variable conductance densities
- Feedback regulation shapes variability to permit temperature robust neural activity
- Robustness to global perturbations constrains cellular regulation mechanisms

eTOC summary

All biochemical processes, including neuronal activity, are temperature sensitive. Yet many animal species experience large temperature fluctuations. O'Leary and Marder show how a simple regulatory control mechanism can ensure temperature robust neural activity by balancing expression of multiple, temperature dependent ion channel types.

Summary

Many species of cold-blooded animals experience substantial and rapid fluctuations in body temperature. Because biological processes are differentially temperature-dependent, it is difficult to understand how physiological processes in such animals can be temperature-robust. [1-8]. Experiments have shown that core neural circuits such as the pyloric circuit of the crab Stomatogastric Ganglion (STG) exhibit robust neural activity in spite of large (20 °C) temperature fluctuations [3, 5, 7, 8]. This robustness is surprising because the temperature dependencies of ionic currents in the STG are not tuned [7]. This is apparently paradoxical because: a) each neuron has many different kinds of ion channels with different temperature dependencies (Q_{10}s) that interact in a highly nonlinear way to produce firing patterns; b) across animals there is substantial variability in conductance densities that nonetheless produce almost identical firing properties. The high variability in conductance densities in these neurons [9, 10] appears to contradict the possibility that robustness is achieved through precise tuning of key temperature-dependent processes. In this paper we develop a theoretical explanation for how temperature robustness can emerge from a simple regulatory control mechanism that is compatible with highly variable conductance densities [11-13]. The resulting model suggests a general mechanism for how nervous systems and excitable tissues can exploit degenerate relationships among temperature-sensitive processes to achieve robust function.

Results

Temperature sensitivity of physiological processes such voltage-dependent ion channel gating are described by an approximate, empirical measure, the Q_{10}, defined as the fold-change per 10 °C from some reference temperature:

$$\frac{R_T}{R_{\text{ref}}} = Q_{10}{}^{(T-T_{\text{ref}})/10} \quad (1)$$

Here R_T is the rate (or magnitude) of the process at temperature T and R_{ref} is the reference value at temperature T_{ref}. A Q_{10} of 1.0 therefore means that a process is temperature-independent. Experimentally, Q_{10}s for single-channel conductance tend to lie in the range of 1.2-1.5. On the other hand, Q_{10}s for ion channel gating or inactivation are typically in the range 2.0 – 4.0 [14], meaning that the rate of channel opening, for example, can speed up more than two-fold per 10 °C increase.

Activity in single neurons and circuits results from the interaction of many nonlinear voltage-gated conductances, and is therefore generically very sensitive to changes in kinetic properties of conductances [4]. This is evident in warm-blooded homeotherms such as humans, where changes in brain temperature of only a few degrees can result in seizures, loss of consciousness or death. Figure 1A illustrates temperature sensitivity in model pacemaker neurons that have been assigned random Q_{10}s over a realistic range (2 - 4). Each neuron has the same set of 8 conductances with fixed densities. At the reference temperature (10 °C) the neurons show identical bursting activity (green traces in Figure 1A). However, this activity is severely disrupted as temperature is varied from 5-25 °C, with each different assignment of Q_{10}s causing qualitatively different changes. In contrast, the biological data reproduced in Figure 1B shows temperature robust pacemaker activity in isolated PD cells of the STG [3]. Notably, the duty cycle of these neurons (the percentage of time the neuron is firing during a burst cycle), which is important for coordinating relative muscle contraction timing, is tightly preserved even though the cycle frequency increases with temperature. Pacemaker duty cycle robustness, in concert with synaptic and intrinsic mechanisms of the follower cells [7], allows temperature compensation of phase relationships in the wider circuit.

Together with other studies [7, 15] the extreme sensitivity of the models in Figure 1A shows that temperature robust behavior is not expected for ion channel Q_{10}s selected from a biologically realistic range. Therefore, some tuning of either the Q_{10}s or the channel densities must occur in temperature-robust biological systems. It is conceivable that ion channel Q_{10}s can be tuned on an evolutionary timescale or on short timescales as a result of protein modification. On the other hand, channel densities are known to be under regulatory control [11-13] and biological data show that conductance expression is highly variable in neurons, including the pacemaker cells of the STG (Figure 1C). This is consistent with theoretical studies that show there are many possible combinations of neuronal parameters consistent with a given type of activity [16-20], suggesting that neurons can somehow find entire families of temperature robust combinations of channel densities.

Temperature robustness via channel density regulation

Consider a physiological property, P, of a neuron – this could be spike frequency, burst duty cycle or any other relevant property. Temperature robustness of P arises when the derivative of P with respect to temperature, T, is close to zero over some temperature range:

$$\frac{dP}{dT} \approx 0$$

For convenience we restrict attention to a single compartment neuron model with fixed capacitance. In this case, all physiological properties depend on the dynamics of the ionic currents in the cell. We can thus write the temperature dependence of P in terms of the temperature-dependence of each current, I_i, using the chain rule [2, 21, 22]:

$$\frac{dP}{dT} = \sum_i \frac{dP}{dI_i}\frac{dI_i}{dT}$$

The contribution of each current, I_i, to P is weighted by the corresponding channel density, $\bar{g}_i$. Thus,

$$\frac{dP}{dT} = \sum_i \bar{g}_i \frac{dP}{dx_i}\frac{dx_i}{dT} \quad (2)$$

where x_i is the unit current due to each channel type (so that $I_i = \bar{g}_i x_i$.) Informally, this relationship can be summarized as:

$$\begin{pmatrix}\text{temperature dependence}\\ \text{of property } P\end{pmatrix} = \sum_{\text{all currents}} \begin{pmatrix}\text{expression level of}\\ \text{current } i\end{pmatrix} \times \begin{pmatrix}\text{change in } P \text{ due to temperature}\\ \text{dependence of current } i\end{pmatrix}$$

Within some range of the $\bar{g}_i$, each current affects membrane potential dynamics to either increase or decrease property P (or it has no effect, in which case it is irrelevant). Therefore, the dP/dx_i terms in (2) are either positive or negative. The dx_i/dT terms depend only on the Q_{10} s corresponding to current i, which are always positive and monotonic. Re-writing equation (2) and setting $dP/dT = 0$, gives:

$$0 = \sum_{i=1}^{n-k} \bar{g}_i \left|\frac{dP}{dx_i}\right| \frac{dx_i}{dT} - \sum_{i=n-k+1}^{n} \bar{g}_i \left|\frac{dP}{dx_i}\right| \frac{dx_i}{dT} \quad (3)$$

Here we have split the currents according to whether dP/dx_i is positive or negative. For a large number, n, of different conductances with a mixture of positive and negative contributions ($1 < k < n$), condition (3) is easily satisfied at a single temperature by solving for $\bar{g}_i$. If, in addition, the dP/dx_i terms are sufficiently smooth, P will be approximately temperature invariant over an extended temperature range. Most importantly, if (3) is satisfied for one set of conductance

densities, $\{\bar{g}_i\}$, then linearly scaled densities $\{\alpha\bar{g}_i\}$ also satisfy (3), where α is a scaling factor. This shows that a single temperature robust solution can extend to entire families of temperature-robust solutions with linearly correlated conductance densities.

Intuitively, the above argument says that temperature robustness is achieved when the temperature dependencies of multiple processes that negatively and positively affect P approximately cancel. This approximate cancelling has been called 'antagonistic balance' [2, 22]. The important point to take from equation (2) is that the weighting of each contribution to overall temperature dependence is controlled by conductance density, equivalently, the expression levels of channel proteins in a biological neuron. Clearly, non-permissive situations can exist, for example if a property depends on only one gating variable of a temperature sensitive conductance.

Equation (3) says that if a property is influenced positively and negatively by multiple temperature-sensitive currents, then temperature robustness can be achieved by controlling conductance densities alone. Furthermore, whenever such solutions exist, linearly correlated temperature-robust sets of conductances will also exist. In neurons that express many types of conductance, there will generally be many positive and negative contributions to a given property, making equation (3) easier to satisfy. Together, this shows that regulation that gives linearly correlated conductances can be sufficient for temperature robustness.

Existence of temperature robust channel density configurations in models with mismatched Q_{10}s

We examined the temperature robustness of duty cycle (fraction of cycle period that the neuron is active) in model bursting pacemaker neurons. Duty cycle is important for coordinating rhythms in central pattern generating circuits, such as in the pyloric circuit of the STG. Moreover, temperature robustness of this property is far from trivial to achieve, as Figure 1A illustrates.

To provide an initial set of candidate models, we randomly sampled conductance densities as well as Q_{10}s in a single compartment conductance based model (Figure 2A). For each sample, all of the voltage-dependent gating variables as well as the unitary conductances and calcium dynamics were assigned random Q_{10} values over a realistic range. Q_{10}s for each gating variable were randomised uniformly in the range ($1< Q_{10} <4$) and unitary conductances in the range (1<

Q_{10} < 1.5). As expected, most (94%) of the 116,400 models we sampled failed to maintain bursting activity over a temperature range (5-25 °C).

However, among the 7013 models that did maintain bursting activity across temperature, 560 (0.5%) of the models maintained duty cycle within a 5% range. The distribution of duty cycle variation in all models over 5-25 °C is shown in Figure 2B, along with the distribution of variation in cycle period. Notably, period is less temperature-robust than duty cycle in these models. Biologically, most neurons and neural circuits, including those found in the pyloric circuit exhibit increases in frequency of bursting or spiking as temperature increases [6-8]. Interestingly, the distribution in duty cycle total variation peaks at 10.5%, very close to the biologically observed value of 13% in isolated pacemaker neurons of the crab pyloric rhythm [3]. Thus, in a neuron with only 8 conductances it is relatively easy to find combinations of Q_{10}s and conductance densities that are temperature robust.

Which conductance parameters contribute to duty cycle robustness? Figure 2C shows histograms of Q_{10} values for which temperature robust bursting (top panel) and temperature robust duty cycle (bottom panel) exist. Permissible Q_{10}s for bursting are broadly distributed, indicating that individual Q_{10} values are relatively unimportant. Some Q_{10}s (colored red) show detectable deviations from uniform distributions, indicating that bursting is sensitive to the corresponding kinetic parameter. These distributions did not alter markedly when we selected parameter sets with robust duty cycles (Fig 2C, lower panel), except for the calcium-dependent potassium conductance, (g_{KCa}), which favored lower Q_{10} values. Therefore, in this model, many combinations of conductances can offset temperature-dependent deviations in kinetics as expected from the previous analysis (Equation 3). As reported previously [15], there was no obvious correlation among the parameters of robust models (data not shown).

Although many sets of conductance densities give rise to temperature robust duty cycle, these represent a small fraction of densities that give temperature robustness of a bursting rhythm to begin with, which in turn occupy a small volume of all feasible conductance densities. Moreover, it is clear that a smaller fraction still (solutions toward the left-hand region of the shaded region of Figure 2B) have temperature robust period as well as duty cycle. In this sample, only two parameter sets can maintain both properties within 10%. Thus, robustness to one property imposes a strong constraint on the ability to be robust to additional properties.

169 Activity-dependent channel regulation can generate temperature robust neuronal properties

170 The fixed conductance densities of the models in Figure 2 allowed us to construct models that
171 regulate their conductances using activity-dependent feedback. We recently showed [11, 12]
172 how a simple model of gene regulation can be coupled to a single, global activity sensor, such as
173 a putative calcium-activated pathway depicted in Figure 3A. Briefly, the expression rates of each
174 gene, m_i, is proportional to the deviation of calcium concentration, $[\mathrm{Ca}]$, from an equilibrium
175 value, Ca_{eq}:

$$\frac{dm_i}{dt} = K_i(\mathrm{Ca}_{eq} - [\mathrm{Ca}]) \qquad (4)$$

176 The origin of Ca_{eq} is discussed extensively in [11] and arises when one considers the interaction
177 between calcium-dependent processes that interact to control gene expression. Together, Ca_{eq},
178 and the expression rate constants, K_i, constitute a regulation parameter set for a model, which
179 is assumed to be fixed for a particular cell type [11, 12]. For example, cells with a constitutively
180 repressed channel gene would have a correspondingly low expression rate. We note that these
181 rates are very slow relative to spikes and calcium oscillations, so these equations effectively
182 average out calcium concentration. Channel densities in the model evolve in proportion to the
183 expression levels of the corresponding genes:

$$\frac{d\bar{g}_i}{dt} = A(m_i - \bar{g}_i) \qquad (5)$$

184 where A is some constant representing channel turnover rate. From random initial conditions,
185 the model settles to a steady-state (ss) in which the channel genes, and thus channel density,
186 are linearly correlated, as can be seen by integrating equations (4-5) and calculating the
187 approximate ratios of the steady state densities, $\bar{g}_i^{ss}$:

$$\bar{g}_i^{ss}/\bar{g}_j^{ss} \approx K_i/K_j \qquad (6)$$

188 further analysis in [11, 12] shows further that this model converges.

189 Equation (6) provides a way to estimate regulation parameters from fixed models. We used the
190 subpopulation of 560 fixed models in Figure 2 that maintained duty cycle within 5% to derive
191 initial guesses for the K_i and the average calcium concentration, Ca_{eq}.

192 Equation (6) is approximate due to nonlinearities between steady-state average calcium and
193 conductance density [11]. We thus sampled regulation parameters in a neighborhood and
194 subjected the resulting self regulating models to temperature perturbations (400 samples for
195 each of the 560 candidate parameter sets, 235,600 in total). In this sample, models are not only
196 required to maintain duty cycle within a 5% range over 5-25 °C, they must also, by necessity,
197 maintain average calcium concentration as temperature changes. A fraction (<1%; 2098
198 parameter sets) satisfied these criteria and generated self-regulating duty cycle-robust neurons.

199 Figure 3B shows the initial and steady-state conductances of an example self-regulating model
200 and its corresponding set of assigned Q_{10} values. Multiple runs of the model generates a
201 population of cells with variable underlying conductances that are linearly correlated [12], as
202 predicted by quation (6). These correlations recapitulate direct measurements of mRNA
203 expression and conductance densities in identified neurons of the STG [9, 10, 13, 23] (Figure 1C).

204 Figure 3C shows membrane potential traces during acute temperature ramps, for five different
205 neurons indicated in Figure 3B (color coded). Figure 3D quantifies duty cycle robustness with
206 respect to temperature in this population of cells. Scaled membrane potential traces of the top
207 cell in Figure 3C are shown in Figure 3E. The action potential waveform in the scale traces
208 deviates with temperature, indicating temperature induced changes in the gating kinetics of the
209 underlying conductances, which is to be expected given the substantial mismatch among the
210 underlying Q_{10}s (Figure 3B). Nonetheless, this set of regulation parameters, along with the other
211 2098 parameter sets, drives conductance densities toward regions of parameter space where
212 temperature effects are balanced to maintain duty cycle.

213 **Discussion**

214 While many sets of conductances and Q_{10}s are temperature robust over some range, these
215 represent a very small fraction of a random sampling of parameter space. Indeed, the
216 conductance densities of successful self-regulating models form a very specific slice through
217 parameter space. The general form of the model we present here demonstrates how a simple,
218 biologically plausible control rule can allow neurons to land in these spaces of “good solutions”
219 where temperature compensation occurs automatically. The signature of this control rule is
220 found in the tight correlations in channel expression that is seen experimentally in temperature
221 robust neurons. We speculate that over evolutionary timescales, the gene sequences and

222 resulting enzymatic interactions that control gene expression have been shaped to make some
223 organisms, tissues and cells acutely temperature robust by similarly constraining the underlying
224 regulatory balance of multiple temperature-dependent components. Although we have focused
225 on the context of rhythmic neuronal activity that is observed to be robust in crustaceans, the
226 principle of how multiple, degenerate temperature-dependent processes can be co-regulated to
227 ensure robustness likely generalizes. For example, many species of cold-blooded homeotherms
228 need to be robust to acute temperature fluctuations in the nervous system so as to maintain
229 thermal homeostasis through the behaviors they employ that demonstrate their temperature
230 preferences [24]. Even commonly used warm-blooded model organisms, such as rodents,
231 exhibit remarkably robust nervous system function in the face of large temperature fluctuations
232 [25]. What remains an open question is how robustness to one perturbation, in this case
233 temperature, can coexist with robustness to other environmental challenges, each of which will
234 potentially impose a new constraint on the available parameters, and thus on the regulatory
235 mechanisms themselves.

236

237 **Experimental Procedures**

238 Single compartment pacemaker model neurons were constructed using channel kinetics
239 described in [12]. The models had 7 voltage-dependent conductances: fast sodium (NaV),
240 transient and slow calcium (CaT, CaS), A-type potassium (KA), calcium-activated potassium
241 (KCa), delayed rectified potassium (Kdr), hyperpolarization-activated mixed cation (Ih) and a
242 leak. Calcium dynamics has a first order decay as described in [12].

243 Temperature dependence was modeled in the time-constants of the channel gating variables,
244 the maximal conductance and the time-constant of calcium buffering. For example, for a
245 conductance g with gating variables, m and h, we have standard kinetic equations $g = \bar{g}m^p h^q$;
246 $\tau_m \dot{m} = m_\infty(V) - m$; $\tau_h \dot{h} = h_\infty(V) - h$, where $\bar{g}$ is maximal conductance, p, q are gating
247 exponents, τ_x are gating time constants, $x_\infty(V)$ are steady-state voltage dependencies and V is
248 membrane potential. The temperature dependence is modeled as $g = R_g(T)\bar{g}m^p h^q$ and
249 $R_m(T)^{-1}\tau_m \dot{m} = m_\infty(V) - m$, (with the same form for h), where T is temperature (in Kelvin)
250 and $R_x(T) = {Q_{10,x}}^{(T-T_{\text{ref}})/10}$. In the case of calcium buffering, the corresponding equation is
251 $R_{\text{Ca}}(T)^{-1}\tau_{\text{Ca}}[\dot{\text{Ca}}] = 0.94 I_{\text{Ca}} - [\text{Ca}] + 0.05$. The coefficient of 0.94 (in units of μM nF / pA) is a

252 geometric factor converting calcium current to concentration assuming the cell is approximated
253 as a cylinder of 50 μm in diameter and 400 μm long and the steady-state value of 0.05 (in μm)
254 corresponds to approximate resting cytosolic calcium concentration [12].

255 Models that use calcium dependent channel regulation (Figure 3) are exactly as described
256 previously [12]. Regulation parameters were chosen as described in the main text. The
257 conductance densities, regulation parameters and Q_{10} values for all simulations are given in
258 table S1 in the supplemental data. Duty cycle measurements were made using a spike threshold
259 of -10mV. Simulation code is available at https://github.com/marderlab/oleary_marder_2016

260 **Acknowledgements**

261 Funding for this work was provided by a Charles A King Trust Fellowship (T.O.) and NIH grants NS
262 081013 and NIH 1P01NS079419 (E.M.)

263 **Author contributions**

264 T.O. conducted research; T.O. and E.M. wrote the paper.

265

References

1. Rajan, K., and Abbott, L.F. (2007). Temperature-compensated chemical reactions. Physical Review E, 75(2), 022902.
2. Hong, C.I., and Tyson, J.J. (1997). A proposal for temperature compensation of the circadian rhythm in Drosophila based on dimerization of the per protein. Chronobiology International *14*, 521-529.
3. Rinberg, A., Taylor, A.L., and Marder, E. (2013). The effects of temperature on the stability of a neuronal oscillator. PLoS computational biology *9*, e1002857.
4. Robertson, R.M., and Money, T.G. (2012). Temperature and neuronal circuit function: compensation, tuning and tolerance. Curr Opin Neurobiol *22*, 724-734.
5. Roemschied, F.A., Eberhard, M.J., Schleimer, J.H., Ronacher, B., and Schreiber, S. (2014). Cell-intrinsic mechanisms of temperature compensation in a grasshopper sensory receptor neuron. Elife *3*, e02078.
6. Soofi, W., Goeritz, M.L., Kispersky, T.J., Prinz, A.A., Marder, E., and Stein, W. (2014). Phase maintenance in a rhythmic motor pattern during temperature changes *in vivo*. J Neurophysiol *111*, 2603-2613.
7. Tang, L., Goeritz, M., Caplan, J., Taylor, A., Fisek, M., and Marder, E. (2010). Precise temperature compensation of phase in a rhythmic motor pattern. PLoS Biol *8*, e1000469.
8. Tang, L.S., Taylor, A.L., Rinberg, A., and Marder, E. (2012). Robustness of a rhythmic circuit to short- and long-term temperature changes. J Neurosci *32*, 10075-10085.
9. Schulz, D.J., Goaillard, J.M., and Marder, E. (2006). Variable channel expression in identified single and electrically coupled neurons in different animals. Nat Neurosci *9*, 356 - 362.
10. Schulz, D.J., Goaillard, J.M., and Marder, E.E. (2007). Quantitative expression profiling of identified neurons reveals cell-specific constraints on highly variable levels of gene expression. Proc Natl Acad Sci USA *104*, 13187-13191.
11. O'Leary, T., Williams, A.H., Caplan, J.S., and Marder, E. (2013). Correlations in ion channel expression emerge from homeostatic tuning rules. Proc Natl Acad Sci USA *110*, E2645-2654.
12. O'Leary, T., Williams, A.H., Franci, A., and Marder, E. (2014). Cell types, network homeostasis, and pathological compensation from a biologically plausible ion channel expression model. Neuron *82*, 809-821.
13. Temporal, S., Lett, K.M., and Schulz, D.J. (2014). Activity-dependent feedback regulates correlated ion channel mRNA levels in single identified motor neurons. Curr Biol *24*, 1899-1904.
14. Hille, B. (2001). Ion channels of excitable membranes, 3rd ed. Edition, (Sinauer).
15. Caplan, J.S., Williams, A.H., and Marder, E. (2014). Many parameter sets in a multicompartment model oscillator are robust to temperature perturbations. J Neurosci *34*, 4963-4975.

16. Golowasch, J., Goldman, M.S., Abbott, L.F., and Marder, E. (2002). Failure of averaging in the construction of a conductance-based neuron model. J Neurophysiol *87*, 1129-1131.
17. Goldman, M.S., Golowasch, J., Marder, E., and Abbott, L.F. (2001). Global structure, robustness, and modulation of neuronal models. J Neurosci *21*, 5229-5238.
18. Taylor, A.L., Goaillard, J.M., and Marder, E. (2009). How multiple conductances determine electrophysiological properties in a multicompartment model. J Neurosci *29*, 5573-5586.
19. Taylor, A.L., Hickey, T.J., Prinz, A.A., and Marder, E. (2006). Structure and visualization of high-dimensional conductance spaces. J Neurophysiol *96*, 891-905.
20. Sobie, E.A. (2009). Parameter sensitivity analysis in electrophysiological models using multivariable regression. Biophysical Journal *96*, 1264-1274.
21. Hong, C.I., Conrad, E.D., and Tyson, J.J. (2007). A proposal for robust temperature compensation of circadian rhythms. Proceedings of the National Academy of Sciences of the United States of America *104*, 1195-1200.
22. Ruoff, P., Rensing, L., Kommedal, R., and Mohsenzadeh, S. (1997). Modeling temperature compensation in chemical and biological oscillators. Chronobiology International *14*, 499-510.
23. Goaillard, J.M., Taylor, A.L., Schulz, D.J., and Marder, E. (2009). Functional consequences of animal-to-animal variation in circuit parameters. Nat Neurosci *12*, 1424-1430.
24. Garrity, P. A., Goodman, M. B., Samuel, A. D., and Sengupta, P. (2010). Running hot and cold: behavioral strategies, neural circuits, and the molecular machinery for thermotaxis in C. elegans and Drosophila. Genes & development, *24*(21), 2365-2382.
25. Moser, E., Mathiesen, I., & Andersen, P. (1993). Association between brain temperature and dentate field potentials in exploring and swimming rats. Science, *259*(5099), 1324-1326.

342 **Figure Legends**

343

344 **Figure 1: Temperature robust neural activity is non-trivial but observed biologically in neurons**
345 **with highly variable conductance expression**
346 (A) Three example model neurons with identical conductance densities and randomly assigned
347 Q_{10}s for all kinetic parameters (values and ranges in Supplemental Table S1). Conductance
348 densities were chosen to produce bursting pacemaker activity at the reference temperature
349 (green traces). All models are subjected to an identical acute temperature ramp between 5 and
350 10 °C and between 10 and 25 °C (blue traces); temperature ramp is shown on the same
351 timescale (red trace). (B) Example traces of a pharmacologically isolated PD pacemaker cell in
352 the STG, subjected to acute changes in temperature, reproduced from [2]. Scale bar spans -75 to
353 -25 mV (vertical) and 1 second (horizontal). (Right) summary measurements of PD duty cycle as
354 a function of temperature across 12 different preparations [1]. (C) Single-cell ion channel gene
355 expression data from PD pacemaker neurons, reproduced from [9]. Units are mRNA copy
356 numbers from single cell real-time PCR, normalized to ribosomal RNA. Blue lines are linear fits
357 where significant correlations were found.

358

359 **Figure 2: Many sets of conductance densities can produce temperature robust neurons with**
360 **mismatched Q_{10}s.**
361 (A) Strategy for sampling temperature-robust combinations of channel densities and Q_{10}s. Both
362 channel densities and Q_{10}s were randomly assigned to 116,400 single compartment models,
363 which were then screened to find temperature robust pacemaking activity by measuring duty
364 cycle and burst period during acute temperature ramps (parameters in Supplemental Table S1).
365 (B) Total variation in cycle period and duty cycle over the temperature range 5 – 25 °C for all
366 7013 models that maintained bursting across temperature. Total variation is defined as the
367 difference between maximum and minimum cycle period/duty cycle across the temperature
368 range. Marginal distributions of period variation and duty cycle variation are shown to the top
369 and right of the plots. Yellow shaded region shows the subset of models that maintained duty
370 cycle within 5% over the temperature range. (C) (Top panel) Histograms of Q_{10}s for all channel
371 gating variables and maximal conductances, and for calcium buffering time-constant and Q_{10}.
372 For maximal conductances, the horizontal axis ranges from 1.0 to 1.5. For calcium buffer time-
373 constant the range is 20-100 ms. For all other Q_{10} histograms the range is 1.0 to 4.0.

Distributions that deviate substantially from the original uniform sampling distribution are shaded red (Kolmogorov-Smirnov statistic > 0.1.) Conductance abbreviations: NaV = fast sodium, CaT = transient calcium, CaS = slow calcium, KA = A-type potassium, KCa = calcium-activated potasium, Kdr = delayer rectifier potassium, Ih = hyperpolarization-activated mixed cation conductance. (Bottom panel) as for Top panel, but for the subset of 560 models that maintained duty cycle within 5%, as depicted in yellow shaded region of (B).

Figure 3. An example of a self-regulating population of model neurons that establish temperature-robust sets of conductance densities

(A) Cartoon of the conductance regulation model used in this paper. Calcium concentration directly modulates the expression rates of all conductances densities by altering the rate of production of a channel intermediate ('mRNA') on an appropriately slow timescale (orders of magnitude slower than fluctuations in calcium due to spikes and membrane potential oscillations). (Lower panel) Example traces showing convergence of the model. Scale bar: 50 mV (vertical), 500 ms (horizontal). See ref [11] for full model details. (B) (Left panel) Random initial conductance densities in 25 model neurons. (Middle panel) Steady-state conductance densities in the same 25 model neurons in the left panel following convergence under the control of one example parameter set from the 2028 parameter sets that produced temperature-robust self-regulating neurons. (Right panel) Q_{10} values of the conductances in the model neurons in the left and middle panels. (C) Acute temperature ramps in five example model neurons selected from the steady-state population in (B). (D) Quantification of duty cycle in the five example neurons in (C) as a function of temperature. (E) Time-stretched membrane potential traces from the blue model neuron in (C).

Supplemental Information

Table S1. Conductance parameters for simulations

Conductance densities (in μS/nF) and Q10 range for model neurons in Figure 1 and ranges for models sampled in Figure 2.

404 **Figure 1**

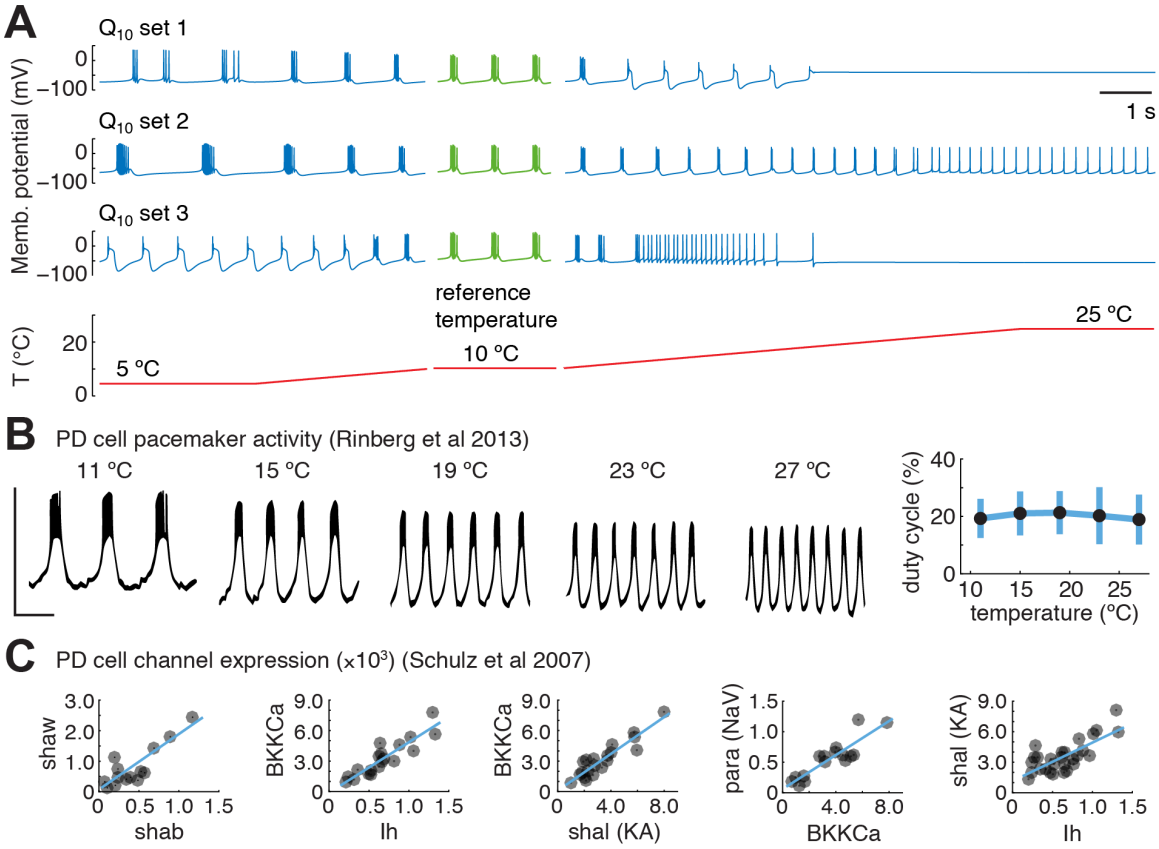

405

406 **Figure 2**

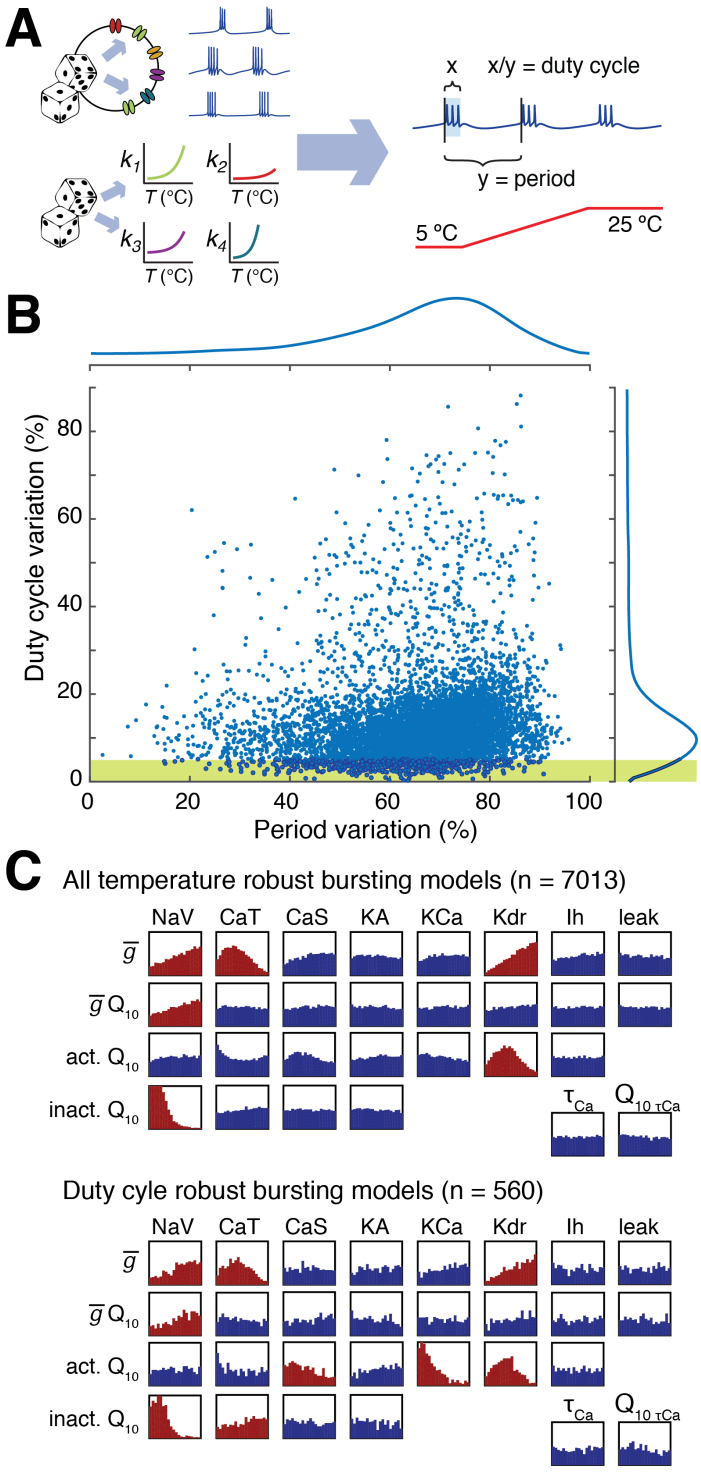

407

408 **Figure 3**

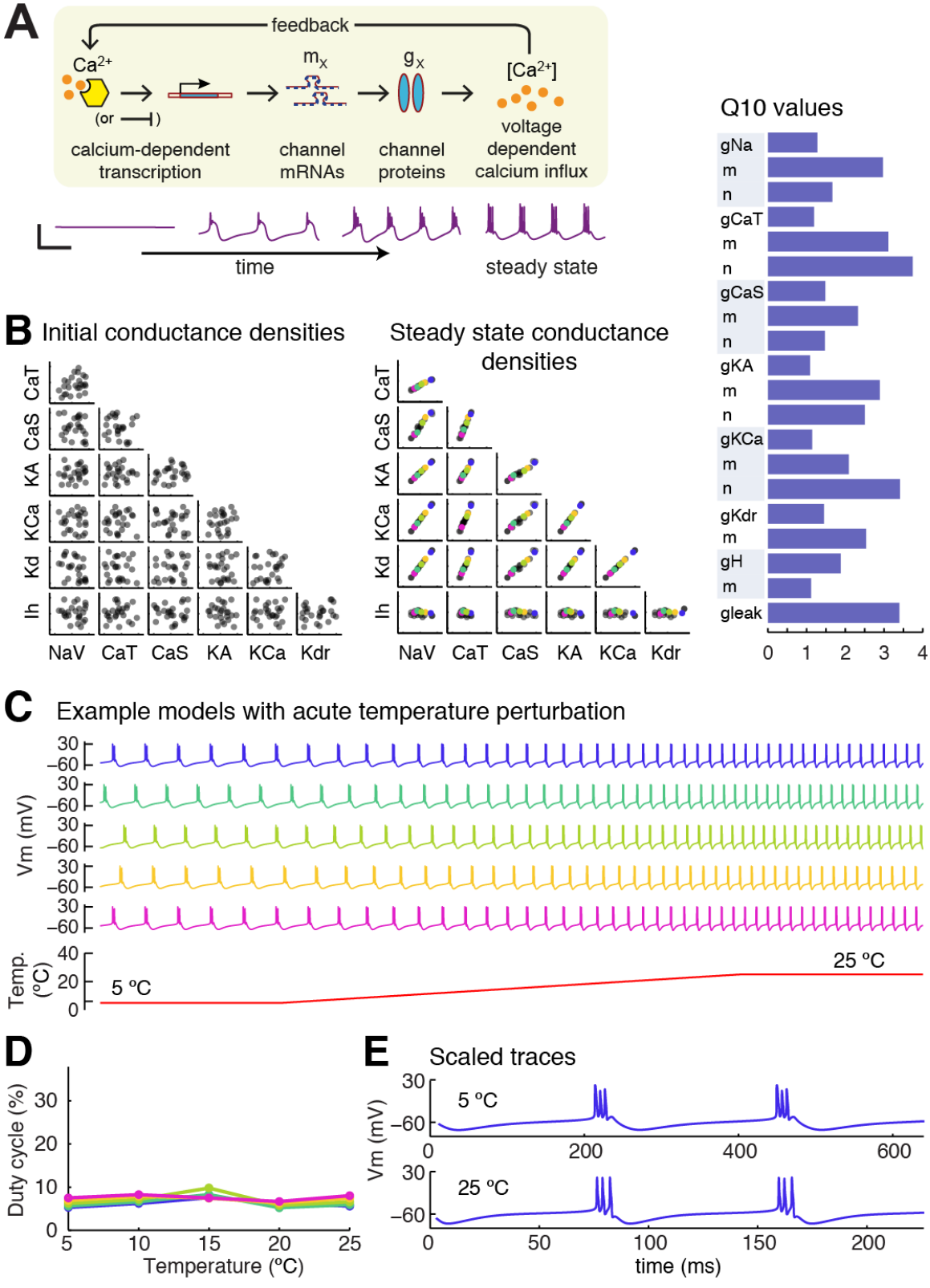

409